

1 **Surface ocean cooling in the Eocene North Atlantic coincides with**
2 **declining atmospheric CO₂**

3
4 Gordon N. Inglis* ⁽¹⁾, Rehemat Bhatia* ⁽²⁾, David Evans ^(1,3), Jiang Zhu⁽⁴⁾, Wolfgang Müller ⁽³⁾, David
5 Matthey ⁽⁵⁾, David Thornalley ⁽⁶⁾, Richard G. Stockey ⁽¹⁾, Bridget S. Wade ⁽²⁾

6
7 (1) School of Ocean and Earth Science, University of Southampton, UK

8 (2) Department of Earth Sciences, University College London, UK

9 (3) Institute of Geosciences, Goethe University Frankfurt, Frankfurt, Germany

10 (4) National Center for Atmospheric Research, Colorado, USA

11 (5) Department of Earth Sciences, Royal Holloway University of London (RHUL), UK

12 (6) Department of Geography, UCL, UK

13
14 * contributed equally to this work

15 Corresponding author: Gordon N. Inglis

16 Email: gordon.inglis@soton.ac.uk. Telephone: +44 (0)117 954 6395

17
18
19
20
21
22
23
24
25
26
27

28 **Key points:**

- 29 • Long-term (~4° C) decline in North Atlantic sea surface temperatures between the early
30 (~53-49 Ma) and middle (~44-41 Ma) Eocene.
- 31 • This indicates that CO₂ was likely responsible for the onset of long-term Eocene cooling.
- 32 • However, east-west temperature gradients in the North Atlantic are decoupled, possibly
33 due to additional non-CO₂ forcing mechanisms.

34

35 **Abstract:**

36 The Eocene (56–34 million years ago) is characterised by declining sea surface temperatures
37 (SSTs) in the low latitudes (~4°C) and high southern latitudes (~8-11°C), in accord with decreasing
38 CO₂ estimates. However, in the mid-to-high northern latitudes there is no evidence for surface
39 water cooling, suggesting thermal decoupling between northern and southern hemispheres and
40 additional non-CO₂ controls. To explore this further, we present a multi-proxy (Mg/Ca, δ¹⁸O, TEX₈₆)
41 SST record from Bass River in the western North Atlantic. Our compiled multi-proxy SST record
42 confirms a net decline in SSTs (~4°C) between the early Eocene Climatic Optimum (53.3-49.1 Ma)
43 and mid-Eocene (~44-41 Ma), supporting declining atmospheric CO₂ as the primary mechanism of
44 Eocene cooling. However, from the mid-Eocene onwards, east-west North Atlantic temperature
45 gradients exhibit different trends, which we attribute to incursion of warmer waters into the eastern
46 North Atlantic and inception of Northern Component Water across the early-middle Eocene
47 transition.

48

49 **Plain Language Summary**

50 Over the past 541 million years, the Earth has oscillated between warm (greenhouse) and cold
51 (icehouse) climates. The most recent transition between a greenhouse and icehouse climate state
52 occurred during the Eocene (56 to 34 million years ago). This transition shows a gradual cooling,
53 previously suggested to be driven by a decline in atmospheric carbon dioxide (CO₂). However, we
54 know little about this transition in the North Atlantic Ocean. Previous studies show limited cooling of

55 surface waters in this region. This suggests that changes in North Atlantic temperatures are not
56 driven by CO₂. To understand how sea surface temperature changes in the western North Atlantic,
57 we analysed the chemistry of microscopic marine fossils in sediments. Our results show a 4°C
58 decline in temperature from the early (~53 Ma) to the middle Eocene (~42 Ma). This matches
59 computer simulations of Eocene climate and confirms CO₂ was responsible for the transition. The
60 lack of cooling observed in previous work is probably due to the development of an ancient water
61 mass known as Northern Component Water (observed today as North Atlantic Deep Water) and
62 changes in how the Eocene ocean transported heat.

63

64 **Introduction**

65 The early Eocene Climatic Optimum (EECO; 53.3 to 49.1 million years ago; Ma) (Hollis et al.,
66 2019a; Zachos et al., 2001) is characterised by a long-term maximum in atmospheric CO₂ (~1470
67 ppm) (Anagnostou et al., 2020), followed by a gradual decline in atmospheric CO₂ during the
68 middle Eocene (47.8 to 38.0 Ma) to ~800ppm (Anagnostou et al., 2020). This is consistent with
69 declining SSTs in the tropics (ca. 4°C) (Cramwinckel et al., 2018; Evans et al., 2018) and the mid-
70 to-high southern latitudes (ca. 8-11 °C; Bijl et al., 2009; Hollis et al., 2009; Hollis et al., 2012).
71 However, SST estimates from the eastern North Atlantic suggest relatively muted surface water
72 cooling (~1°C) between the EECO and middle Eocene (~40 Ma) (Bornemann et al., 2016).
73 Temperature asymmetry between the northern and southern hemisphere would not be expected
74 from a long-term decline in atmospheric CO₂ alone (Liu et al., 2018) and suggests that other non-
75 CO₂ driving mechanisms (e.g. gateway reorganisation and/or changes in ocean circulation) may
76 influence regional SST patterns.

77 Of particular relevance is the growing evidence for Northern Component Water (NCW)
78 initiation in the North Atlantic during the early-middle Eocene (~49 and 47 Ma) (Boyle et al., 2017;
79 Hohbein et al., 2012; Norris et al., 2001). The onset of NCW has been attributed to gateway
80 reorganisation, specifically deepening of the Greenland-Scotland Ridge (GSR) (Boyle et al., 2017;
81 Hohbein et al., 2012; Vahlenkamp et al., 2018), although other mechanisms have been proposed

82 such as isolation of the Arctic Ocean (Zhang et al., 2011) or restriction of the Tethys Ocean
83 (Roberts et al., 2009). The onset of NCW is followed by a period of weaker overturning (~42 to 38
84 Ma) (Witkowski et al., 2021), before re-invigoration of NCW during the late Eocene (~38 Ma)
85 (Coxall et al., 2018) or Eocene-Oligocene transition (EOT; ~34 Ma) (Hutchinson et al., 2019). The
86 establishment of NCW can transport additional heat into the eastern North Atlantic (Vahlenkamp et
87 al., 2018), potentially muting any long-term cooling trend in this region and has been invoked to
88 explain stable temperatures in the eastern North Atlantic during the middle Eocene (Bornemann et
89 al., 2016). However, our understanding of long-term North Atlantic temperature change is based on
90 a single proxy record (planktonic foraminiferal $\delta^{18}\text{O}$) from a single site (DSDP Site 401; Bornemann
91 et al., 2016) and may not be regionally representative.

92 To test whether the wider North Atlantic region exhibits stable temperatures during the
93 Eocene, we use a multi-proxy approach ($\delta^{18}\text{O}$, Mg/Ca, TEX_{86}) to reconstruct SST in the western
94 North Atlantic (Bass River; ODP Leg 174AX; ~36°N paleolatitude) during the early-to-middle
95 Eocene (53.7 to 42.0 Ma). We compare our new dataset with climate model simulations spanning
96 a wide range of CO_2 values to explore (i) temporal and spatial patterns of cooling in the North
97 Atlantic during the Eocene and (ii) whether there is thermal decoupling between the northern and
98 southern hemisphere during the Eocene. This allows us to test whether declining CO_2 is the
99 primary driver of long-term Eocene cooling or whether regional forcing mechanisms are also
100 important.

101

102 **Methods**

103 *Site description*

104 The Bass River section (ODP Leg 174AX; 39°36'N, 74°26'W) consists of calcareous marls and
105 glauconitic silty clays deposited in middle to outer neritic paleodepths between 30 and 150 m
106 (Fung et al., 2019; Miller et al., 2003). The biostratigraphic age model was developed using
107 planktonic foraminifera and nannofossils (following Fung et al., 2019) with datums converted to the
108 GTS2012 (Vandenbergh et al., 2012). Sediments span the early to middle Eocene (53.7 to 42.0

109 Ma) and encompass the EECO (~340 to 291 m). However, there are a series of hiatuses between
110 ~49 and 44 Ma.

111

112 *Analytical methods*

113 Lipid biomarker analysis was performed on 47 sediment samples. Approximately 5-10g of
114 sediment was extracted with an Ethos Ex microwave extraction system using 15 ml of
115 dichloromethane (DCM) and methanol (MeOH) (9:1, v/v). The total lipid extract was separated over
116 silica into apolar and polar fractions using hexane:dichloromethane (9:1, v/v) and
117 dichloromethane:methanol (1:2, v/v), respectively. The polar fraction (containing isoGDGTs) was
118 dissolved in hexane/isopropanol (99:1, v/v), passed through 0.45µm PTFE filters and analysed by
119 HPLC/APCI-MS following Hopmans et al. (2016). Trace element and stable oxygen isotope ($\delta^{18}\text{O}$)
120 planktonic foraminiferal analysis was performed on multiple depth intervals (n = 8) spanning the
121 early-to-middle Eocene. Foraminiferal preservation is excellent, appearing transparent or
122 translucent under the light microscope, with no signs of diagenetic alteration observed under SEM
123 (**Figure S1; Table S1**). Analysis was performed on various surface-dwelling species
124 (*Acarinina praetopilensis*, *Morozovella formosa*, *Morozovelloides crassatus*, and
125 *Pseudohastigerina wilcoxensis*) and deeper, thermocline-dwelling species (*Parasubbotina hagni*,
126 *Parasubbotina inaequispira*). Single-specimen Mg/Ca analysis was performed via slow depth-
127 profiling by laser ablation-inductively coupled mass spectrometry (LA-ICPMS) (see Müller et al.,
128 2009; Supplementary Information; **Table S2**). Mg/Ca values were determined in multiple chambers
129 (~3 to 5) within a single specimen and averaged. The same specimens were subsequently
130 analysed for $\delta^{18}\text{O}$ using a Multiprep-Isoprime 100 dual inlet system optimised for analysis of single
131 specimens (Supplementary information).

132

133 *Temperature calibrations*

134 TEX_{86} data was screened using established indices for non-Thaumarchaeota inputs
135 (Supplementary Information; **Figure S5**) and converted to SST using a Bayesian linear calibration
136 (prior mean = 25, prior standard deviation = 10, n = 2000) (Tierney and Tingley, 2014). Planktonic

137 foraminiferal $\delta^{18}\text{O}$ values were converted to SST using the bayfox Bayesian calibration (prior mean
138 = 25, prior standard deviation = 20, $n = 2000$). Seawater $\delta^{18}\text{O}$ ($\delta^{18}\text{O}_{\text{sw}}$) values were obtained via
139 the isotope-enabled Community Earth System Model version 1.2 (iCESM1.2; see below). Mg/Ca
140 values were converted into SST using a modified version of MgCaRB (Gray and Evans, 2019)
141 (Supplementary Information). We report pH-corrected Mg/Ca temperatures as the majority of
142 modern foraminifer species are characterised by Mg/Ca-pH sensitivity (Gray and Evans, 2019).
143 Planktonic foraminifera were rare and thus for Mg/Ca and $\delta^{18}\text{O}$, we report the 'average' SST
144 estimates for a given time slice ($n = 8$ for $\delta^{18}\text{O}$, $n = 7$ for Mg/Ca) by combining (i) multiple-
145 specimens from multiple size fractions and (ii) all surface-dwelling species within multiple genera
146 (i.e., *Acarinina praetopilensis*, *Acarinina pseudotopilensis*, *Morozovella formosa*, *Morozovelloides*
147 *crassatus*, *Pseudohastigerina wilcoxensis*) into a single estimate, following DeepMIP protocols
148 (Hollis et al, 2019; Supplementary Information). Average 'SST' estimates comprise a minimum of
149 two samples from a single depth horizon (see **Data S4-S5**). When SSTs are calculated using
150 individual species (**Figure S2**) and size segregating species (**Figure S2-S3**), similar patterns in
151 long-term trends are observed.

152

153 *Climate model simulations*

154 We use the water isotope-enabled Community Earth System Model version 1.2 (iCESM1.2) (Zhu
155 et al., 2020; Zhu et al., 2019) to compare with our proxy reconstruction and to provide an
156 independent estimate of $\delta^{18}\text{O}_{\text{sw}}$. iCESM1.2 is able to closely replicate large-scale features of early
157 Eocene climate, including: i) enhanced global mean surface temperature estimates (Lunt et al.,
158 2021; Zhu et al., 2019), ii) reduced meridional temperature gradients (Lunt et al., 2021), iii)
159 changes in the hydrological cycle (Cramwinckel et al., 2023), and iv) the values and distribution of
160 planktonic foraminifera $\delta^{18}\text{O}$ values (Zhu et al., 2020). It is also the only DeepMIP model that has
161 water isotopes enabled (Zhu et al., 2020). The iCESM1.2 simulations were performed following the
162 Deep-time Model Intercomparison Project protocols (Lunt et al., 2017) with early Eocene
163 paleogeography and vegetation (56.0–47.8 Ma) (Herold et al., 2014) and atmospheric CO_2 levels

164 of x1, x3, x6, and x9 preindustrial values (284.7 ppmv). Seawater $\delta^{18}\text{O}$ in the simulations was
165 initialized from a constant value of -1.0‰ to account for the absence of ice sheets in a hothouse
166 climate (Shackleton and Kennett, 1975; Hollis et al., 2019). Previous studies at Bass River have
167 suggested sea level changes through the middle Eocene on the order of 20-30 m, that have been
168 attributed to changes in Antarctic ice volume (Fung et al., 2019). We do not adjust $\delta^{18}\text{O}_{\text{sw}}$ in this
169 study for middle Eocene ice volume fluctuations, as the timing and magnitude of these ephemeral
170 glaciations are currently poorly constrained and our planktonic $\delta^{18}\text{O}$ data from Bass River are from
171 intervals where water depth was greatest (i.e. ice volume was minimal). Our model results indicate
172 only minor changes in $\delta^{18}\text{O}_{\text{sw}}$ at the Bass River location through the early-middle Eocene ($\sim 0.2\text{‰}$
173 change between x1 and x9 CO_2 simulations using iCESM1.2; **Table S3**). As such, we use the
174 average $\delta^{18}\text{O}_{\text{sw}}$ value (-0.54‰) to calculate planktonic foraminiferal $\delta^{18}\text{O}$ -derived SST estimates.
175 See Zhu et al. (2019; 2020) and Zhang et al. (2022) for further details of the experimental setup
176 and equilibration state.

177

178 **Results**

179 During the EECO (53.3 to 49.1 Ma), TEX_{86} SST estimates average $\sim 33^\circ\text{C}$ (**Figure 1a**). Between
180 the EECO and the middle Eocene (44-41 Ma), TEX_{86} SST estimates decline by $\sim 5^\circ\text{C}$ (**Figure 1a**).
181 Oxygen isotope SST estimates during the EECO from surface-dwelling planktonic foraminifera
182 average $\sim 32^\circ\text{C}$ (**Figure 1a**). Surface-dwelling species yield higher temperatures (up to $\sim 5^\circ\text{C}$
183 higher) than thermocline-dwelling species but exhibit a similar magnitude of cooling ($\sim 4^\circ\text{C}$)
184 between the EECO and the middle Eocene (44-41 Ma). During the early Eocene, Mg/Ca SST
185 estimates (calculated using the *G. ruber* calibration) average $\sim 27^\circ\text{C}$ (**Figure 1a**). These values are
186 lower than $\delta^{18}\text{O}$ and TEX_{86} SST estimates by $\sim 5^\circ\text{C}$ and $\sim 6^\circ\text{C}$, respectively; **Figure 1a**) but agree
187 within the propagated calibration uncertainties. Mg/Ca SST estimates increase by $\sim 3^\circ\text{C}$ between
188 the EECO and middle Eocene (44-41 Ma; **Figure 1a**). However, the absolute values ($\sim 30^\circ\text{C}$) are
189 comparable to middle Eocene-aged TEX_{86} and $\delta^{18}\text{O}$ SST estimates (28°C and 29°C , respectively)
190 and agree within the propagated calibration uncertainties.

191

192 **Discussion**

193 *Long-term cooling in the western North Atlantic during the Eocene*

194 The use of multiple proxies provides more robust long-term temperature records than a single
195 proxy. The consistency between Mg/Ca, oxygen isotopes and TEX₈₆ values in the EECO and late
196 Eocene is encouraging and indicates that each proxy is recording the same environmental signal
197 (i.e. SST). TEX₈₆ and δ¹⁸O values indicate very high SSTs at Bass River during the EECO (~32 to
198 33°C). These values are in agreement with existing low-resolution TEX₈₆ estimates generated at
199 Bass River (de Bar et al., 2019) and nearby South Dover Bridge (~34°C; Inglis et al., 2015). Mg/Ca
200 SST estimated are also relatively high (~27°C; **Figure 1**) but are lower than TEX₈₆ and δ¹⁸O-
201 derived SST estimates by ~5-6°C. Between the EECO and middle Eocene (44-41 Ma), TEX₈₆ and
202 δ¹⁸O values indicate gradual surface water cooling (5 and 4°C, respectively; **Figure 1a**), coherent
203 with declining TEX₈₆ SSTs (~7°C) at South Dover Bridge between the EECO and middle Eocene
204 (~42 Ma). Evidence of cooling in two independent proxies (TEX₈₆, δ¹⁸O) and locations provides the
205 first compelling evidence for surface ocean cooling in the (western) North Atlantic between the
206 early and middle Eocene, which is in parallel with the inferred deep-ocean cooling in benthic
207 foraminifera δ¹⁸O record (Figure 1b; Westerhold et al., 2020).

208 In contrast, our new Mg/Ca SSTs increase by ~3°C between the EECO and middle
209 Eocene. Although middle Eocene (44-41 Ma) SST estimates are in excellent agreement with TEX₈₆
210 and δ¹⁸O values (**Figure 1**) and alkenone-derived SST estimates (~29-30°C; Liu et al, 2018) from
211 nearby site IODP Site 1404, the temporal trends are inconsistent with regional observations (*this*
212 *paper*) (de Bar et al., 2019; Inglis et al., 2015) and declining global bottom water temperature
213 estimates inferred via changes in benthic foraminiferal δ¹⁸O values (Figure 1b) (Westerhold et al.,
214 2020). To explore this mismatch further, we compared our proxy-derived temperature estimates
215 (TEX₈₆, Mg/Ca, δ¹⁸O) from the EECO (53.3 to 49.1 Ma; Hollis et al. 2019) and middle Eocene (44
216 to 41 Ma) alongside iCESM1.2 simulations with different CO₂ scenarios (x1 to x9 pre-industrial
217 CO₂) (**Figure S6**). These two intervals are chosen as they contain SST estimates from multiple

218 proxies (Mg/Ca, $\delta^{18}\text{O}$ and TEX_{86}) and exhibit a similar sampling density. iCESM1.2 simulated SSTs
219 at the Bass River are 31 and 27 °C in the x6 and x3 PI CO_2 simulations, respectively (**Figure 2b**),
220 which overlaps with proxy reconstructions (**Figure 2a**; **Figure S6**). For a two-fold decrease in
221 atmospheric CO_2 (i.e., from x6 to x3 PI CO_2), the model predicted decrease in SST of $\sim 4^\circ\text{C}$ is
222 comparable to the magnitude of cooling captured by TEX_{86} and $\delta^{18}\text{O}$ (5 and 4 °C, respectively;
223 **Figure S6**) between the EECO and middle Eocene, but is inconsistent with warming observed in
224 Mg/Ca values. Given that proxy-derived CO_2 estimates decline from ~ 1470 ppm (\sim x5 PI CO_2) to
225 ~ 800 ppm (\sim x3 PI CO_2) during this interval (Anagnostou et al., 2020), this implies additional non-
226 thermal controls on Mg/Ca values at this site.

227 The choice of Mg/Ca calibration remains uncertain when working with extinct species.
228 However, the discrepancy between Mg/Ca-derived SSTs and other proxy data is insensitive to the
229 choice of Mg/Ca calibration approach (Supplementary Information). This is because seawater pH
230 was substantially lower than modern throughout the Eocene (Anagnostou et al., 2020), such that
231 choosing a *G. ruber* or *T. sacculifer*-like calibration has a minor effect on the long-term Mg/Ca-
232 derived trend in our dataset (**Figure S3**). Seawater Mg/Ca is also well-constrained for the Eocene
233 (Evans et al., 2018; Gothmann et al., 2015) and is broadly invariant across this interval, such that it
234 is very unlikely that unidentified changes mask cooling. Given that this site was targeted for its
235 exceptional foraminiferal preservation and diverse assemblages (**Figure S1**), this potentially points
236 towards either an evolutionary control on Eocene planktonic foraminifera Mg incorporation, or a
237 shift in seawater carbonate chemistry at this site that substantially differs from the existing pH
238 records (Anagnostou et al., 2020; Rae et al., 2021; see Supplementary Information for more
239 discussion). Resolving this issue and exploring any other additional controls (e.g., local
240 hydrographic variability; c.f. Thornalley et al., 2011) will require further data and is beyond the
241 scope of this study. We continue to include the Mg/Ca SST estimates in our assessment of the
242 thermal evolution of Bass River (**Figure 2a**) and note that mismatches in $\delta^{18}\text{O}$ and Mg/Ca derived
243 SSTs are not unique to deep-time species. Furthermore, this discrepancy in inorganic geochemical
244 temperature reconstructions may ultimately stem from a small number of Mg/Ca analyses in the

245 early Eocene, highlighting the benefit of working with a larger numbers of specimens, where
246 possible.

247

248 *Divergent zonal temperature gradients in the North Atlantic during the early-to-middle Eocene*

249 To determine the long-term mean SST evolution at Bass River, we fit LOESS regressions to our
250 multi-proxy dataset (TEX₈₆, Mg/Ca, $\delta^{18}\text{O}$) (Supplementary Information). This approach indicates
251 net cooling ($\sim 4^\circ\text{C}$) in the western North Atlantic between the EECO and middle Eocene (**Figure**
252 **2a**). Our data from the western North Atlantic contrasts with existing planktonic foraminifera $\delta^{18}\text{O}$ -
253 derived SST estimates from the eastern North Atlantic ($\sim 37^\circ\text{N}$; DSDP Site 401; Bornemann et al.,
254 2016) that indicate minimal ($< 1^\circ\text{C}$) or no cooling between the EECO and late middle Eocene (ca.
255 42-40 Ma) (**Figure 2a**). CESM1.2 model simulations show that the magnitude of cooling at Bass
256 River inferred via proxies is consistent with a halving of CO_2 (**Figure 2c**) but that the magnitude of
257 proxy-inferred cooling at DSDP Site 401 is much lower than expected (**Figure 2b-c**). The east-
258 west zonal mean temperature gradient inferred via proxy estimates ($\sim 15\text{-}20^\circ\text{C}$) is also larger than
259 inferred via model simulations ($\sim 3^\circ\text{C}$; **Figure 2b**). As the model simulations are identical with the
260 exception of changes in CO_2 , this implies that non- CO_2 controls influence SSTs in the eastern
261 North Atlantic (DSDP Site 401; Bornemann et al., 2016) during the Eocene.

262 Planktonic foraminifera at Bass River exhibit excellent preservation (Supplementary
263 Information) and tests are translucent and 'glassy' (Figure S1) whereas Hollis et al. (2019)
264 classified post-PETM planktonic foraminifera at DSDP Site 401 as 'recrystallized'. However, post-
265 PETM foraminifera at DSDP Site 401 exhibit good preservation (Bornemann et al., 2016) and show
266 limited evidence for recrystallization. If planktonic foraminifera had been subject to significant post-
267 depositional alteration, they would be "reset" towards deep-sea temperatures and would track
268 changes in benthic foraminiferal $\delta^{18}\text{O}$ values (Pearson et al., 2007). However, planktonic
269 foraminiferal $\delta^{18}\text{O}$ values at DSDP Site 401 do not co-vary with benthic $\delta^{18}\text{O}$ values, either at this
270 site (Bornemann et al., 2016) or elsewhere (Westerhold et al., 2020). Therefore, this is unlikely to

271 explain the observed trends (**Figure 2a**). However, additional SST records from the North Atlantic
272 are required to explore regional variations further.

273 Alternatively, changes in ocean circulation could have modulated regional temperature
274 patterns in the eastern North Atlantic during the middle-to-late Eocene, specifically the onset of
275 Northern Component Water (NCW) formation. None of the DeepMIP models (including CESM1.2)
276 show deep overturning circulation (> 2,000 m) in the North Atlantic during the early Eocene (Zhang
277 et al., 2022), consistent with proxy evidence (e.g., benthic foraminifera $\delta^{13}\text{C}$ and fish teeth ϵ_{Nd}
278 values; see Zhang et al. (2022). Instead, most of the DeepMIP models (and CESM simulations
279 with 1x to 3x CO_2) suggests that deep water formation is likely to form in the Southern Ocean,
280 which also broadly agrees with proxy-based evidence from the early Eocene (Zhang et al., 2022).
281 CESM does simulate a North Atlantic deep/intermediate water formation at 1x PI CO_2 , suggesting
282 that NCW formation represents a delicate balance between multiple factors such as global or
283 regional cooling, widening of the Atlantic basin, closure of the Arctic-Atlantic gateway (Hutchinson
284 et al., 2019) and/or deepening/opening of the Greenland-Scotland Ridge (Vahlenkamp et al., 2018;
285 Straume et al., 2022). The lack of deep water formation in iCESM1.2 at high CO_2 concentrations
286 (i.e. 6x CO_2) is likely related to the initial condition and short integration length (see Zhang et al.,
287 2022 for further discussion). We speculate that this limitation in the iCESM1.2 simulation at 6x CO_2
288 would have a minor impact on the surface ocean of the North Atlantic, where regional ocean-
289 atmosphere coupling and wind driven circulation are more important in determining the SSTs.

290 Idealised modelling experiments show that deepening of the Greenland-Scotland Ridge
291 and/or closure of the Arctic-Atlantic gateway (Hutchinson et al., 2019) can initiate NCW formation
292 in the North Atlantic and increase SST in the eastern North Atlantic by up to 7 °C (Vahlenkamp et
293 al., 2018), thus muting any long-term CO_2 -driven cooling at DSDP Site 401. Importantly, deepening
294 of the Greenland-Scotland Ridge has only a minimal influence (< 1°C) on SSTs in the western
295 North Atlantic (i.e., where Bass River is located) (Vahlenkamp et al., 2018). There is growing
296 geochemical and sedimentological evidence placing the initial onset of NCW between ~49 and 47
297 Ma, coincident with changes in zonal temperature gradients between the eastern and western
298 North Atlantic. Evidence for onset of NCW between ~49 and 47 Ma includes development of

299 contourite drifts in the western North Atlantic (Boyle et al., 2017), changes in biosiliceous
300 sedimentation (Witkowski et al., 2021) and a collapse in $\delta^{13}\text{C}$ gradients between the North and
301 South Atlantic (Hohbein et al., 2012). These changes would also influence local hydrography within
302 the eastern North Atlantic and could exert an additional control on $\delta^{18}\text{O}_{\text{sw}}$ values at DSDP Site 401.

303 Proxy-based reconstructions during the Middle Eocene Climatic Optimum have argued that
304 northward expansion of the North Atlantic subtropical gyre could also act as a mechanism to
305 increase SSTs within the North Atlantic (Van Der Ploeg et al., 2023). However, details of the gyre
306 heat transport and the impact of this large-scale process on regional SSTs (especially near
307 coastlines) requires further investigation. Thus, although diverging zonal temperature gradients in
308 the North Atlantic are consistent with the initial early onset of NCW during the early-middle Eocene,
309 additional proxy data and isotope-enabled model simulations are required to test this further. From
310 a model-based perspective, simulations with higher resolution and longer simulation length are
311 required to explore the equilibrium state of the modelled ocean circulation and any possible
312 regional features that may be missed by the relatively coarse ($\sim 1\text{--}2^\circ$) resolution model.

313
314 *Synchronous surface water cooling in the northern and southern hemispheres during the Eocene*

315 To explore whether long-term cooling is globally synchronous, we compiled TEX_{86} -derived SST
316 estimates that span the early (55 Ma) to late (34 Ma) Eocene. To avoid relying on single proxy
317 records, we focus on regions with two or more TEX_{86} records. Our data compilation spans three
318 regions: (i) the equatorial Atlantic ($0\text{--}30^\circ$ N/S) (Cramwinckel et al., 2018; Zhang et al., 2013; Inglis
319 et al., 2015; Liu et al., 2009), (ii) the northwest Atlantic ($30\text{--}50^\circ$ N) (*this study*; Keating-Bitonti et al.,
320 2011; Inglis et al., 2015; Cramwinckel et al., 2020a; van der Ploeg et al., 2023) and (iii) the
321 southwest Pacific ($>50^\circ$ S) (Bijl et al., 2013; Bijl et al., 2009; Crouch et al., 2020; Hollis et al., 2009;
322 Inglis et al., 2015; Cramwinckel et al., 2020b; Liu et al., 2009). (**Figure 3**; Supplementary
323 Information).

324 Our results suggest that the onset of long-term cooling occurs ~ 49 to 48 million years ago
325 in the North Atlantic and southwest Pacific (i.e. following the termination of the EECO; **Figure 3a-c**)
326 and coincides with an increase in the latitudinal SST gradient from 49 to 44 Ma (**Figure 3d**). Our

327 study indicates that the onset of Eocene cooling is a global feature and thus consistent with a
328 decline in atmospheric CO₂ as a forcing mechanism for cooling. However, there is a relative lack of
329 data in the North Atlantic from ~49 to 48 Ma, such that additional records are required to determine
330 the exact onset of long-term cooling. Proxy records have also suggested that ocean gateways may
331 have played an important role at this time (e.g., Hohbein et al., 2012; Bijl et al., 2009; Bijl et al.,
332 2013). Previous work argues that the Tasman Gateway was open to shallow circulation at this time
333 (~49 to 46 Ma) (Bijl et al., 2013) and deepening of the Tasman Gateway would initiate regional
334 surface water cooling (Sijp et al., 2011; Sijp et al., 2016) and may account for declining SSTs in the
335 SW Pacific between the termination of the EECO and middle Eocene (~44 Ma). However, as
336 surface ocean cooling occurs in multiple basins (Figure 3a-c) at a comparable time (~49-48 Ma), it
337 suggests that CO₂ was likely responsible for the majority of long-term Eocene cooling.

338

339 **Conclusions**

340 Here we present the first multi-proxy (Mg/Ca, $\delta^{18}\text{O}$, TEX₈₆) SST record from the western North
341 Atlantic spanning the early-to-middle Eocene. Our results indicate very high SSTs during the early
342 Eocene Climatic Optimum (~27-33°C), in agreement with high atmospheric CO₂ concentrations.
343 Our compiled dataset reveal a net decline (~4°C) in SSTs between the early Eocene Climatic
344 Optimum (53.3-49.1 Ma) and the middle Eocene (44-41 Ma), consistent with long-term decrease in
345 atmospheric CO₂. However, east-west zonal temperature gradients in the North Atlantic are likely
346 decoupled during the early-to-middle Eocene. This may be related to inception of Northern
347 Component Water at the early-middle Eocene transition and incursion of warmer waters into the
348 eastern North Atlantic, but additional datasets are required to test this further. We also
349 demonstrate that the onset of long-term Eocene cooling in the western North Atlantic (~49-48 Ma)
350 occurs synchronously in other ocean basins (e.g., N. Atlantic vs S. Pacific) and across different
351 latitudinal bands, implying that CO₂ was likely responsible for the onset of long-term Eocene
352 cooling.

353

354 **Acknowledgements**

355 Samples were provided by IODP which is sponsored by the NSF and participating countries. GNI
356 was supported by a Royal Society Dorothy Hodgkin Fellowship (DHF\R1\191178) and NERC
357 (NE/V018388/1). We thank NEIF-B for analytical support and Jim Davy for SEM imaging support.
358 RB acknowledges funding from a NERC PhD studentship (no. 1352360), the Cushman Foundation
359 for Foraminiferal Research (Joseph A. Cushman Award for Student Research), and a 2016
360 Geologists' Association New Researchers' Award. BW was supported by NERC (NE/V018361/1,
361 NE/G014817). LA-ICPMS work at RHUL was partly funded by a 2014 NERC Capital Equipment
362 Grant (CC073) to WM. The CESM project is supported primarily by the National Science
363 Foundation (NSF). This material is based upon work supported by the National Center for
364 Atmospheric Research, a major facility sponsored by the NSF under Cooperative Agreement No.
365 1852977. JZ was supported by NSF Grant 2202777. We thank Jim Browning for information on the
366 age model and Tianchen He for support in trace element and isotope data interpretation. We thank
367 David Hutchinson and two anonymous reviewers whose thoughtful comments significantly
368 improved the manuscript.

369 **Open Research**

370 Inorganic and organic geochemical data and associated sea surface temperature estimates are
371 available at OSF (Inglis et al., 2023). The transformation of measured Mg/Ca into temperature was
372 calculated using MgCaRB (Evans et al., 2023). Loess regressions were calculated using R
373 (<http://www.R-project.org>).

374

375 **Captions**

376

377 **Figure 1. a)** SST reconstructions from Bass River during the early-middle Eocene inferred via
378 TEX₈₆ (blue), planktonic foraminifera $\delta^{18}\text{O}$ (dark orange) and Mg/Ca (light orange). Error bars
379 represent the 95% confidence intervals. b) Atmospheric CO₂ reconstructions inferred via planktonic
380 foraminifera $\delta^{11}\text{B}$ (blue circles) and alkenone $\delta^{13}\text{C}$ (blue squares). Error bars represent ± 1 standard
381 deviation (Rae et al., 2021). c) benthic foraminifera $\delta^{18}\text{O}$ values (Westerhold et al., 2020).

382

383 **Figure 2:** Divergent zonal temperature gradients in the North Atlantic during the early-to-middle
384 Eocene. a) proxy-derived SST reconstructions for Bass River (*this study*; blue symbols) and DSDP
385 Site 401 ($\delta^{18}\text{O}$ only; orange symbols) (Bornemann et al., 2016) fitted with a LOESS regression.
386 $\delta^{18}\text{O}$ values from DSDP Site 401 re-calculated for surface-dwelling foraminiferal genera (*Acarinina*
387 *and Morozovella* spp.) using the bayfox Bayesian calibration ($\delta^{18}\text{O}_{\text{sw}} = -0.81$, prior mean = 25, prior
388 standard deviation = 20, $n = 2000$). $\delta^{18}\text{O}_{\text{sw}}$ values obtained via iCESM1.2 (Table S3). Error bars
389 represent the 95% confidence intervals. b) iCESM1.2-derived SST estimates for Bass River (blue
390 symbols) and DSDP Site 401 (orange symbols) under different CO_2 concentrations, c) iCESM1.2-
391 derived ΔSST estimates ($\times 6 \text{ PI CO}_2 - \times 3 \text{ PI CO}_2$) with proxy-derived cooling between the early- to
392 middle Eocene shown for each site

393

394 **Figure 3:** Long-term evolution of surface ocean temperatures during the Eocene inferred via TEX_{86}
395 in the (a) equatorial Atlantic (Cramwinckel et al., 2018; Inglis et al., 2015; Zhang et al., 2013), b)
396 North Atlantic (*this study*; Inglis et al., 2015; de Bar et al., 2019), and c) the southwest Pacific (Bijl
397 et al., 2013; Bijl et al., 2009; Crouch et al., 2020; Hollis et al., 2009; Inglis et al., 2015). Panel (d)
398 shows the SST gradient between the equatorial Atlantic and the North Atlantic (dark blue line) and
399 southwest Pacific (light blue line). To determine the long-term mean SST evolution for the low-,
400 mid-, and high-latitudes, nonparametric LOESS regressions were fitted using the fANCOVA
401 software package (<http://www.R-project.org/>).

402

403 **References**

404 Anagnostou, E., John, E. H., Babila, T., Sexton, P., Ridgwell, A., Lunt, D. J., Pearson, P. N., Chalk,
405 T., Pancost, R. D., and Foster, G., 2020, Proxy evidence for state-dependence of climate
406 sensitivity in the Eocene greenhouse: *Nature Communications*, v. 11, no. 1, p. 1-9.

407 Barker, S., Cacho, I., Benway, H., and Tachikawa, K., 2005, Planktonic foraminiferal Mg/Ca as a
408 proxy for past oceanic temperatures: a methodological overview and data compilation for
409 the Last Glacial Maximum: *Quaternary Science Reviews*, v. 24, no. 7-9, p. 821-834.

410 Bijl, P. K., Bendle, J. A. P., Bohaty, S. M., Pross, J., Schouten, S., Tauxe, L., Stickley, C. E.,
411 McKay, R. M., Röhl, U., Olney, M., Sluijs, A., Escutia, C., Brinkhuis, H., and Scientists, E.,
412 2013, Eocene cooling linked to early flow across the Tasmanian Gateway: Proceedings of
413 the National Academy of Sciences, v. 110, no. 24, p. 9645-9650.

414 Bijl, P. K., Schouten, S., Sluijs, A., Reichart, G.-J., Zachos, J. C., and Brinkhuis, H., 2009, Early
415 Palaeogene temperature evolution of the southwest Pacific Ocean: Nature, v. 461, no.
416 7265, p. 776-779.

417 Bornemann, A., D'haenens, S., Norris, R. D., and Speijer, R. P., 2016, The demise of the early
418 Eocene greenhouse—Decoupled deep and surface water cooling in the eastern North
419 Atlantic: Global and Planetary Change, v. 145, p. 130-140.

420 Bornemann, A., Norris, R. D., Lyman, J. A., D'Haenens, S., Groeneveld, J., Röhl, U., Farley, K. A.,
421 and Speijer, R. P., 2014, Persistent environmental change after the Paleocene–Eocene
422 Thermal Maximum in the eastern North Atlantic: Earth and Planetary Science Letters, v.
423 394, p. 70-81.

424 Boyle, P. R., Romans, B. W., Tucholke, B. E., Norris, R. D., Swift, S. A., and Sexton, P. F., 2017,
425 Cenozoic North Atlantic deep circulation history recorded in contourite drifts, offshore
426 Newfoundland, Canada: Marine Geology, v. 385, p. 185-203.

427 Coxall, H. K., Huck, C. E., Huber, M., Lear, C. H., Legarda-Lisarri, A., O'regan, M., Sliwiska, K. K.,
428 Van De Fliedert, T., De Boer, A. M., and Zachos, J. C., 2018, Export of nutrient rich Northern
429 Component Water preceded early Oligocene Antarctic glaciation: Nature Geoscience, v.
430 11, no. 3, p. 190-196.

431 Cramwinckel, M. J., Huber, M., Kocken, I. J., Agnini, C., Bijl, P. K., Bohaty, S. M., Frieling, J.,
432 Goldner, A., Hilgen, F. J., and Kip, E. L., 2018, Synchronous tropical and polar temperature
433 evolution in the Eocene: Nature, v. 559, no. 7714, p. 382-386.

434 Cramwinckel, M.J., Coxall, H.K., Śliwińska, K.K., Polling, M., Harper, D.T., Bijl, P.K., Brinkhuis, H.,
435 Eldrett, J.S., Houben, A.J., Peterse, F. and Schouten, S., 2020. A warm, stratified, and
436 restricted Labrador Sea across the middle Eocene and its climatic
437 optimum. *Paleoceanography and Paleoclimatology*, 35(10), p.e2020PA003932.

438 Cramwinckel, M.J., Burls, N.J., Fahad, A.A., Knapp, S., West, C.K., Reichgelt, T., Greenwood,
439 D.R., Chan, W.L., Donnadieu, Y., Hutchinson, D.K. de Boer, A.M., Ladant, J.B., Morozova,
440 P., Niezgodski, I., Knorr, G., Steinig, S., Zhang, Z., Zhu., J., Feng, R., Lunt, D.J., Abe-
441 Ouchi, A., and Inglis, G.N. 2023. Global and zonal-mean hydrological response to early
442 Eocene warmth. *Paleoceanography and Paleoclimatology*, p.e2022PA004542.

443 Crouch, E., Shepherd, C., Morgans, H., Naafs, B., Dallanave, E., Phillips, A., Hollis, C., and
444 Pancost, R. D., 2020, Climatic and environmental changes across the early Eocene climatic
445 optimum at mid-Waipara River, Canterbury Basin, New Zealand: *Earth-Science Reviews*, v.
446 200, p. 102961.

447 de Bar, M., de Nooijer, L., Schouten, S., Ziegler, M., Sluijs, A., and Reichert, G. J., 2019,
448 Comparing seawater temperature proxy records for the past 90 Myrs from the shallow shelf
449 record Bass River, New Jersey: *Paleoceanography and Paleoclimatology*, v. 34, no. 4, p.
450 455-475.

451 Evans, D., Sahoo, N., Renema, W., Cotton, L. J., Müller, W., Todd, J. A., Saraswati, P. K.,
452 Stassen, P., Ziegler, M., and Pearson, P. N., 2018, Eocene greenhouse climate revealed
453 by coupled clumped isotope-Mg/Ca thermometry: *Proceedings of the National Academy of*
454 *Sciences*, v. 115, no. 6, p. 1174-1179.

455 Evans, D. 2023. dbjevans/MgCaRB: v1.0 (v1.0). Zenodo. [software]
456 <https://doi.org/10.5281/zenodo.10200630>

457 Fung, M. K., Katz, M. E., Miller, K. G., Browning, J. V., and Rosenthal, Y., 2019, Sequence
458 stratigraphy, micropaleontology, and foraminiferal geochemistry, Bass River, New Jersey
459 paleoshelf, USA: Implications for Eocene ice-volume changes: *Geosphere*, v. 15, no. 2, p.
460 502-532.

461 Gothmann, A. M., Stolarski, J., Adkins, J. F., Schoene, B., Dennis, K. J., Schrag, D. P., Mazur, M.,
462 and Bender, M. L., 2015, Fossil corals as an archive of secular variations in seawater
463 chemistry since the Mesozoic: *Geochimica et Cosmochimica Acta*, v. 160, p. 188-208.

464 Gray, W. R., and Evans, D., 2019, Nonthermal influences on Mg/Ca in planktonic foraminifera: A
465 review of culture studies and application to the last glacial maximum: *Paleoceanography*
466 and *Paleoclimatology*, v. 34, no. 3, p. 306-315.

467 Herold, N., Buzan, J., Seton, M., Goldner, A., Green, J., Müller, R., Markwick, P., and Huber, M.,
468 2014, A suite of early Eocene (~ 55 Ma) climate model boundary conditions: *Geoscientific*
469 *Model Development*.

470 Hohbein, M. W., Sexton, P. F., and Cartwright, J. A., 2012, Onset of North Atlantic Deep Water
471 production coincident with inception of the Cenozoic global cooling trend: *Geology*, v. 40,
472 no. 3, p. 255-258.

473 Hollis, C. J., Dunkley Jones, T., Anagnostou, E., Bijl, P. K., Cramwinckel, M. J., Cui, Y., Dickens,
474 G. R., Edgar, K. M., Eley, Y., and Evans, D., 2019a, The DeepMIP contribution to PMIP4:
475 methodologies for selection, compilation and analysis of latest Paleocene and early Eocene
476 climate proxy data, incorporating version 0.1 of the DeepMIP database: *Geoscientific Model*
477 *Development*, v. 12, no. 7, p. 3149-3206.

478 Hollis, C. J., Dunkley Jones, T., Anagnostou, E., Bijl, P. K., Cramwinckel, M. J., Cui, Y., Dickens,
479 G. R., Edgar, K. M., Eley, Y., Evans, D., Foster, G. L., Frieling, J., Inglis, G. N., Kennedy, E.
480 M., Kozdon, R., Lauretano, V., Lear, C. H., Littler, K., Lourens, L., Meckler, A. N., Naafs, B.
481 D. A., Pälike, H., Pancost, R. D., Pearson, P. N., Röhl, U., Royer, D. L., Salzmann, U.,
482 Schubert, B. A., Seebeck, H., Sluijs, A., Speijer, R. P., Stassen, P., Tierney, J., Tripathi, A.,
483 Wade, B.S., Westerhold, T., Witkowski, C., Zachos, J. C., Zhang, Y. G., Huber, M., and
484 Lunt, D. J., 2019b, The DeepMIP contribution to PMIP4: methodologies for selection,
485 compilation and analysis of latest Paleocene and early Eocene climate proxy data,
486 incorporating version 0.1 of the DeepMIP database: *Geosci. Model Dev.*, v. 12, no. 7, p.
487 3149-3206.

488 Hollis, C. J., Handley, L., Crouch, E. M., Morgans, H. E., Baker, J. A., Creech, J., Collins, K. S.,
489 Gibbs, S. J., Huber, M., and Schouten, S., 2009, Tropical sea temperatures in the high-
490 latitude South Pacific during the Eocene: *Geology*, v. 37, no. 2, p. 99-102.

491 Hollis, C. J., Taylor, K. W. R., Handley, L., Pancost, R. D., Huber, M., Creech, J. B., Hines, B. R.,
492 Crouch, E. M., Morgans, H. E. G., Crampton, J. S., Gibbs, S., Pearson, P. N., and Zachos,
493 J. C., 2012, Early Paleogene temperature history of the Southwest Pacific Ocean:
494 Reconciling proxies and models: *Earth and Planetary Science Letters*, v. 349–350, no. 0, p.
495 53-66.

496 Hopmans, E. C., Schouten, S., and Damsté, J. S. S., 2016, The effect of improved
497 chromatography on GDGT-based palaeoproxies: *Organic Geochemistry*, v. 93, p. 1-6.

498 Hutchinson, D. K., Coxall, H. K., O'Regan, M., Nilsson, J., Caballero, R., and de Boer, A. M., 2019,
499 Arctic closure as a trigger for Atlantic overturning at the Eocene-Oligocene Transition:
500 *Nature Communications*, v. 10, no. 1, p. 3797.

501 Inglis, G. N., Farnsworth, A., Lunt, D., Foster, G. L., Hollis, C. J., Pagani, M., Jardine, P. E.,
502 Pearson, P. N., Markwick, P., Galsworthy, A. M. J., Raynham, L., Taylor, K. W. R., and
503 Pancost, R. D., 2015, Descent toward the icehouse; Eocene sea surface cooling inferred
504 from GDGT distributions: *Paleoceanography*, v. 30, no. 7, p. 1000.

505 Inglis, G.N. (2023) Surface ocean cooling in the Eocene North Atlantic coincides with declining
506 atmospheric CO₂ [dataset] 10.17605/OSF.IO/BGTRU

507 Inglis, G. N., and Tierney, J. E., 2020, *The TEX86 Paleotemperature Proxy*, Cambridge University
508 Press.

509 Keating-Bitonti, C.R., Ivany, L.C., Affek, H.P., Douglas, P. and Samson, S.D., 2011. Warm, not
510 super-hot, temperatures in the early Eocene subtropics. *Geology*, 39(8), pp.771-774.

511 Liu, Z., He, Y., Jiang, Y., Wang, H., Liu, W., Bohaty, S. M., and Wilson, P. A., 2018, Transient
512 temperature asymmetry between hemispheres in the Palaeogene Atlantic Ocean: *Nature*
513 *Geoscience*, v. 11, no. 9, p. 656-660.

514 Lunt, D. J., Bragg, F., Chan, W.-L., Hutchinson, D. K., Ladant, J.-B., Morozova, P., Niezgodzki, I.,
515 Steinig, S., Zhang, Z., Zhu, J., Abe-Ouchi, A., Anagnostou, E., de Boer, A. M., Coxall, H. K.,
516 Donnadieu, Y., Foster, G., Inglis, G. N., Knorr, G., Langebroek, P. M., Lear, C. H.,
517 Lohmann, G., Poulsen, C. J., Sepulchre, P., Tierney, J. E., Valdes, P. J., Volodin, E. M.,
518 Dunkley Jones, T., Hollis, C. J., Huber, M., and Otto-Bliesner, B. L.: DeepMIP: model

519 intercomparison of early Eocene climatic optimum (EECO) large-scale climate features and
520 comparison with proxy data, *Clim. Past*, 17, 203–227, [https://doi.org/10.5194/cp-17-203-](https://doi.org/10.5194/cp-17-203-2021)
521 2021, 2021

522 Lunt, D. J., Huber, M., Anagnostou, E., Baatsen, M. L. J., Caballero, R., DeConto, R., Dijkstra, H.
523 A., Donnadieu, Y., Evans, D., Feng, R., Foster, G. L., Gasson, E., von der Heydt, A. S.,
524 Hollis, C. J., Inglis, G. N., Jones, S. M., Kiehl, J., Kirtland Turner, S., Korty, R. L., Kozdon,
525 R., Krishnan, S., Ladant, J.-B., Langebroek, P., Lear, C. H., LeGrande, A. N., Littler, K.,
526 Markwick, P., Otto-Bliesner, B., Pearson, P., Poulsen, C. J., Salzmann, U., Shields, C.,
527 Snell, K., Stärz, M., Super, J., Tabor, C., Tierney, J. E., Tourte, G. J. L., Tripathi, A.,
528 Upchurch, G. R., Wade, B. S., Wing, S. L., Winguth, A. M. E., Wright, N. M., Zachos, J. C.,
529 and Zeebe, R. E.: The DeepMIP contribution to PMIP4: experimental design for model
530 simulations of the EECO, PETM, and pre-PETM (version 1.0), *Geosci. Model Dev.*, 10,
531 889–901, <https://doi.org/10.5194/gmd-10-889-2017>, 2017.

532 Meckler, A. N., Sexton, P., Piasecki, A., Leutert, T., Marquardt, J., Ziegler, M., Agterhuis, T.,
533 Lourens, L., Rae, J., and Barnet, J., 2022, Cenozoic evolution of deep ocean temperature
534 from clumped isotope thermometry: *Science*, v. 377, no. 6601, p. 86-90.

535 Miller, K. G., Sugarman, P. J., Browning, J. V., Olsson, R. K., Pekar, S. F., Reilly, T. J., Cramer, B.
536 S., Aubry, M.-P., Lawrence, R. P., Curran, J., Stewart, M., Metzger, J. M., Uptegrove, J.,
537 Bukry, D., Burckle, L. H., Wright, J. D., Feigenson, M. D., Brenner, G. J., and Dalton, R. F.,
538 1998. Bass River Site. *Proceedings of the Ocean Drilling Program, Initial Reports*, 174AX,
539 5-43.

540 Miller, K. G., Browning, J. V., Sugarman, P. J., McLaughlin, P. P., Kominz, M. A., Olsson, R. K.,
541 Wright, J. D., Cramer, B. S., Pekar, S., and Van Sickle, W., 2003, 174AX Leg summary:
542 Sequences, sea level, tectonics, and aquifer resources: Coastal plain drilling: *Proceedings*
543 *of Ocean Drilling Program, Initial Reports*, 174AX (Suppl.)(Ed. by KG Miller, PJ Sugarman
544 & JV Browning, et al.) p. 1-40.

545 Müller, W., Shelley, M., Miller, P., and Broude, S., 2009, Initial performance metrics of a new
546 custom-designed ArF excimer LA-ICPMS system coupled to a two-volume laser-ablation
547 cell: *Journal of Analytical Atomic Spectrometry*, v. 24, no. 2, p. 209-214.

548 Norris, R., Klaus, A., and Kroon, D., 2001, Mid-Eocene deep water, the late Palaeocene thermal
549 maximum and continental slope mass wasting during the Cretaceous-Palaeogene impact:
550 Geological Society, London, Special Publications, v. 183, no. 1, p. 23-48.

551 Pearson, P.N., van Dongen, B.E., Nicholas, C.J., Pancost, R.D., Schouten, S., Singano, J.M. and
552 Wade, B.S., 2007. Stable warm tropical climate through the Eocene Epoch. *Geology*, 35(3),
553 pp.211-214.

554 Rae, J.W., Zhang, Y.G., Liu, X., Foster, G.L., Stoll, H.M. and Whiteford, R.D., 2021. Atmospheric
555 CO₂ over the past 66 million years from marine archives. *Annual Review of Earth and*
556 *Planetary Sciences*, 49, pp.609-641.

557 Roberts, C. D., LeGrande, A. N., and Tripathi, A. K., 2009, Climate sensitivity to Arctic seaway
558 restriction during the early Paleogene: *Earth and Planetary Science Letters*, v. 286, no. 3-4,
559 p. 576-585.

560 Shackleton, N.J. and Kennett, J.P. 1975. Paleotemperature history of the Cenozoic and the
561 initiation of Antarctic glaciation: oxygen and carbon isotope analyses in DSDP Sites 277,
562 279, and 281. *Initial Reports Deep Sea Drilling Project*, 29, p.743-755.

563 Sijp, W. P., England, M. H., and Huber, M., 2011, Effect of the deepening of the Tasman Gateway
564 on the global ocean: *Paleoceanography*, v. 26, no. 4.

565 Sijp, W. P., von der Heydt, A. S., and Bijl, P. K., 2016, Model simulations of early westward flow
566 across the Tasman Gateway during the early Eocene: *Climate of the Past*, v. 12, no. 4, p.
567 807-817.

568 Straume, E.O., Nummelin, A., Gaina, C. and Nisancioglu, K.H., 2022. Climate transition at the
569 Eocene–Oligocene influenced by bathymetric changes to the Atlantic–Arctic oceanic
570 gateways. *Proceedings of the National Academy of Sciences*, 119(17), p.e2115346119.

571 Tierney, J. E., and Tingley, M. P., 2014, A Bayesian, spatially-varying calibration model for the
572 TEX₈₆ proxy: *Geochimica et Cosmochimica Acta*, v. 127, p. 83-106.

573 Vahlenkamp, M., Niezgodzki, I., De Vleeschouwer, D., Lohmann, G., Bickert, T., and Pälike, H.,
574 2018, Ocean and climate response to North Atlantic seaway changes at the onset of long-
575 term Eocene cooling: *Earth and Planetary Science Letters*, v. 498, p. 185-195.

576 Vandenberghe, N., Hilgen, F. J., Speijer, R. P., 2012. The Paleogene Period. In: Gradstein, F.,
577 Ogg, J., Schmitz, M., Ogg, G. (eds.), *The Geological Time Scale 2012*. Elsevier,
578 Amsterdam, 855–921.

579 Van Der Ploeg, R., Cramwinckel, M. J., Kocken, I. J., Leutert, T. J., Bohaty, S. M., Fokkema, C. D.,
580 Hull, P. M., Meckler, A. N., Middelburg, J. J., and Müller, I. A., 2023, North Atlantic surface
581 ocean warming and salinization in response to middle Eocene greenhouse warming:
582 *Science advances*, v. 9, no. 4, p. eabq0110.

583 Westerhold, T., Marwan, N., Drury, A. J., Liebrand, D., Agnini, C., Anagnostou, E., Barnet, J. S.,
584 Bohaty, S. M., De Vleeschouwer, D., and Florindo, F., 2020, An astronomically dated
585 record of Earth's climate and its predictability over the last 66 million years: *Science*, v. 369,
586 no. 6509, p. 1383-1387.

587 Witkowski, J., Bryłka, K., Bohaty, S. M., Mydłowska, E., Penman, D. E., and Wade, B. S., 2021,
588 North Atlantic marine biogenic silica accumulation through the early to middle Paleogene:
589 implications for ocean circulation and silicate weathering feedback: *Climate of the Past*, v.
590 17, no. 5, p. 1937-1954.

591 Zachos, J., Pagani, M., Sloan, L., Thomas, E. and Billups, K., 2001. Trends, rhythms, and
592 aberrations in global climate 65 Ma to present. *science*, 292(5517), pp.686-693.

593 Zhang, Y. G., Pagani, M., Liu, Z., Bohaty, S. M., and DeConto, R., 2013, A 40-million-year history
594 of atmospheric CO₂: *Philosophical Transactions of the Royal Society A: Mathematical,*
595 *Physical and Engineering Sciences*, v. 371, no. 2001.

596 Zhang, Z., Nisancioglu, K. H., Flatøy, F., Bentsen, M., Bethke, I., and Wang, H., 2011, Tropical
597 seaways played a more important role than high latitude seaways in Cenozoic cooling:
598 *Climate of the Past*, v. 7, no. 3, p. 801-813.

599 Zhu, J., Poulsen, C. J., Otto-Bliesner, B. L., Liu, Z., Brady, E. C., and Noone, D. C., 2020,
600 Simulation of early Eocene water isotopes using an Earth system model and its implication
601 for past climate reconstruction: *Earth and Planetary Science Letters*, v. 537, p. 116164.
602 Zhu, J., Poulsen, C. J., and Tierney, J. E., 2019, Simulation of Eocene extreme warmth and high
603 climate sensitivity through cloud feedbacks: *Science Advances*, v. 5, no. 9, p. eaax1874.

604

605 **Supplementary Information References:**

606 Barker, S., Cacho, I., Benway, H., & Tachikawa, K. (2005). Planktonic foraminiferal Mg/Ca as a
607 proxy for past oceanic temperatures: a methodological overview and data compilation for
608 the Last Glacial Maximum. *Quaternary Science Reviews*, 24(7-9), 821-834.

609 Evans, D., Brierley, C., Raymo, M.E., Erez, J., Müller, W., (2016). Planktic foraminifera shell
610 chemistry response to seawater chemistry: Pliocene–Pleistocene seawater Mg/Ca,
611 temperature and sea level change. *Earth and Planetary Science Letters* 438, 139–148.
612 <https://doi.org/10.1016/j.epsl.2016.01.013>

613 Evans, D., Erez, J., Oron, S., Müller, W., (2015a). Mg/Ca-temperature and seawater-test chemistry
614 relationships in the shallow-dwelling large benthic foraminifera *Operculina ammonoides*.
615 *Geochimica et Cosmochimica Acta* 148, 325–342.
616 <https://doi.org/10.1016/j.gca.2014.09.039>

617 Evans, D., Bhatia, R., Stoll, H., & Müller, W. (2015b). LA-ICPMS Ba/Ca analyses of planktic
618 foraminifera from the Bay of Bengal: Implications for late Pleistocene orbital control on
619 monsoon freshwater flux. *Geochemistry, Geophysics, Geosystems*, 16(8), 2598-2618.

620 Evans, D., Müller, W., (2012). Deep time foraminifera Mg/Ca paleothermometry: Nonlinear
621 correction for secular change in seawater Mg/Ca. *Paleoceanography* 27.
622 <https://doi.org/10.1029/2012PA002315>

623 Evans, D., & Müller, W. (2018). Automated extraction of a five-year LA-ICP-MS trace element data
624 set of ten common glass and carbonate reference materials: Long-term data quality,

625 optimisation and laser cell homogeneity. *Geostandards and Geoanalytical Research*, 42(2),
626 159-188.

627 Evans, D., Sahoo, N., Renema, W., Cotton, L.J., Müller, W., Todd, J.A., Saraswati, P.K., Stassen,
628 P., Ziegler, M., Pearson, P.N., Valdes, P.J., Affek, H.P., (2018). Eocene greenhouse
629 climate revealed by coupled clumped isotope-Mg/Ca thermometry. *PNAS* 115, 1174–1179.
630 <https://doi.org/10.1073/pnas.1714744115>

631 Fung, M.K., Katz, M.E., Miller, K.G., Browning, J.V. and Rosenthal, Y., 2019. Sequence
632 stratigraphy, micropaleontology, and foraminiferal geochemistry, Bass River, New Jersey
633 paleoshelf, USA: Implications for Eocene ice-volume changes. *Geosphere*, 15(2), pp.502-
634 532.

635 Gray, W.R., Evans, D., (2019). Nonthermal Influences on Mg/Ca in Planktonic Foraminifera: A
636 Review of Culture Studies and Application to the Last Glacial Maximum. *Paleoceanography*
637 and *Paleoclimatology* 34, 306–315. <https://doi.org/10.1029/2018PA003517>

638 Holland, K., Branson, O., Haynes, L.L., Hönisch, B., Allen, K.A., Russell, A.D., Fehrenbacher, J.S.,
639 Spero, H.J., Eggins, S.M., (2020). Constraining multiple controls on planktic foraminifera
640 Mg/Ca. *Geochimica et Cosmochimica Acta* 273, 116–136.
641 <https://doi.org/10.1016/j.gca.2020.01.015>

642 Hollis, C.J., Dunkley Jones, T., Anagnostou, E., Bijl, P.K., Cramwinckel, M.J., Cui, Y., Dickens,
643 G.R., Edgar, K.M., Eley, Y., Evans, D. and Foster, G.L., 2019. The DeepMIP contribution to
644 PMIP4: Methodologies for selection, compilation and analysis of latest Paleocene and early
645 Eocene climate proxy data, incorporating version 0.1 of the DeepMIP
646 database. *Geoscientific Model Development*, 12(7), pp.3149-3206.

647 Hönisch, B., Allen, K.A., Lea, D.W., Spero, H.J., Eggins, S.M., Arbuszewski, J., deMenocal, P.,
648 Rosenthal, Y., Russell, A.D., Elderfield, H., (2013). The influence of salinity on Mg/Ca in
649 planktic foraminifers – Evidence from cultures, core-top sediments and complementary

650 $\delta^{18}O$. *Geochimica et Cosmochimica Acta* 121, 196–213.
651 <https://doi.org/10.1016/j.gca.2013.07.028>

652 Hopmans, E.C., Weijers, J.W., Schefuß, E., Herfort, L., Damsté, J.S.S. and Schouten, S., 2004. A
653 novel proxy for terrestrial organic matter in sediments based on branched and isoprenoid
654 tetraether lipids. *Earth and Planetary Science Letters*, 224(1-2), pp.107-116.

655 Inglis, G.N., Farnsworth, A., Lunt, D., Foster, G.L., Hollis, C.J., Pagani, M., Jardine, P.E., Pearson,
656 P.N., Markwick, P., Galsworthy, A.M. and Raynham, L., 2015. Descent toward the
657 Icehouse: Eocene sea surface cooling inferred from GDGT
658 distributions. *Paleoceanography*, 30(7), pp.1000-1020.

659 Jochum, K. P., Stoll, B., Herwig, K., Willbold, M., Hofmann, A. W., Amini, M., ... & Woodhead, J. D.
660 (2006). MPI-DING reference glasses for in situ microanalysis: New reference values for
661 element concentrations and isotope ratios. *Geochemistry, Geophysics, Geosystems*, 7(2).

662 Kim, J.H., Van der Meer, J., Schouten, S., Helmke, P., Willmott, V., Sangiorgi, F., Koç, N.,
663 Hopmans, E.C. and Damsté, J.S.S., 2010. New indices and calibrations derived from the
664 distribution of crenarchaeal isoprenoid tetraether lipids: Implications for past sea surface
665 temperature reconstructions. *Geochimica et Cosmochimica Acta*, 74(16), pp.4639-4654.

666 Longerich, H. P., Jackson, S. E., & Günther, D. (1996). Inter-laboratory note. Laser ablation
667 inductively coupled plasma mass spectrometric transient signal data acquisition and
668 analyte concentration calculation. *Journal of analytical atomic spectrometry*, 11(9), 899-
669 904.

670 Miller, K.G., Kominz, M.A., Browning, J.V., Wright, J.D., Mountain, G.S., Katz, M.E., Sugarman,
671 P.J., Cramer, B.S., Christie-Blick, N., Pekar, S.F., (2005). The Phanerozoic Record of
672 Global Sea-Level Change. *Science* 310, 1293–1298.
673 <https://doi.org/10.1126/science.1116412>

674 Miller, K.G., Sugarman, P.J., Browning, J.V., Kominz, M.A., Hernández, J.C., Olsson, R.K., Wright,
675 J.D., Feigenson, M.D. and Van Sickle, W., 2003. Late Cretaceous chronology of large,

676 rapid sea-level changes: Glacioeustasy during the greenhouse world. *Geology*, 31(7),
677 pp.585-588.

678 Mucci, A., Morse, J.W., (1983). The incorporation of Mg²⁺ and Sr²⁺ into calcite overgrowths:
679 influences of growth rate and solution composition. *Geochimica et Cosmochimica Acta* 47,
680 217–233. [https://doi.org/10.1016/0016-7037\(83\)90135-7](https://doi.org/10.1016/0016-7037(83)90135-7)

681 Müller, W., Shelley, M., Miller, P., & Broude, S. (2009). Initial performance metrics of a new
682 custom-designed ArF excimer LA-ICPMS system coupled to a two-volume laser-ablation
683 cell. *Journal of Analytical Atomic Spectrometry*, 24(2), 209-214.

684 Pearson, P. N., Olsson, R. K., Huber, B. T., Hemleben, C., & Berggren, W. A. (2006). Atlas of
685 Eocene planktonic foraminifera. Cushman Foundation for Foraminiferal Research. Special
686 Publication (No. 41).

687 Rae, J.W.B., Zhang, Y.G., Liu, X., Foster, G.L., Stoll, H.M., Whiteford, R.D.M., (2021). Atmospheric
688 CO₂ over the Past 66 Million Years from Marine Archives. *Annual Review of Earth and*
689 *Planetary Sciences* 49, 609–641. <https://doi.org/10.1146/annurev-earth-082420-063026>

690 Rattanasriampaipong, R., Zhang, Y.G., Pearson, A., Hedlund, B.P. and Zhang, S., 2022. Archaeal
691 lipids trace ecology and evolution of marine ammonia-oxidizing archaea. *Proceedings of*
692 *the National Academy of Sciences*, 119(31), p.e2123193119.

693 Spratt, R.M., Lisiecki, L.E., (2016). A Late Pleistocene sea level stack. *Climate of the Past* 12,
694 1079–1092. <https://doi.org/10.5194/cp-12-1079-2016>

695 Taylor, K.W., Huber, M., Hollis, C.J., Hernandez-Sanchez, M.T. and Pancost, R.D., 2013. Re-
696 evaluating modern and Palaeogene GDGT distributions: Implications for SST
697 reconstructions. *Global and Planetary Change*, 108, pp.158-174.

698 Tierney, J.E. and Tingley, M.P., 2014. A Bayesian, spatially-varying calibration model for the
699 TEX86 proxy. *Geochimica et Cosmochimica Acta*, 127, pp.83-106.

700 Westerhold, T., Marwan, N., Drury, A.J., Liebrand, D., Agnini, C., Anagnostou, E., Barnet, J.S.K.,
701 Bohaty, S.M., Vleeschouwer, D.D., Florindo, F., Frederichs, T., Hodell, D.A., Holbourn,
702 A.E., Kroon, D., Lauretano, V., Littler, K., Lourens, L.J., Lyle, M., Pälike, H., Röhl, U., Tian,
703 J., Wilkens, R.H., Wilson, P.A., Zachos, J.C., (2020). An astronomically dated record of
704 Earth's climate and its predictability over the last 66 million years. *Science*.

705 Wit, J. C., Reichert, G.-J., A Jung, S. J., and Kroon, D. Approaches to unravel seasonality in sea
706 surface temperatures using paired single-specimen foraminiferal d18O and Mg/Ca
707 analyses. *Paleoceanography*, 25(4), 2010. ISSN 1944-9186. doi: 10.1029/2009PA001857.
708 URL <http://dx.doi.org/10.1029/2009PA001857>. PA4220.

709 Zeebe, R.E. and Tyrrell, T., 2019. History of carbonate ion concentration over the last 100 million
710 years II: Revised calculations and new data. *Geochimica et Cosmochimica Acta*, 257,
711 pp.373-392.

712 Zhang, Y.G., Zhang, C.L., Liu, X.L., Li, L., Hinrichs, K.U. and Noakes, J.E., 2011. Methane Index:
713 A tetraether archaeal lipid biomarker indicator for detecting the instability of marine gas
714 hydrates. *Earth and Planetary Science Letters*, 307(3-4), pp.525-534.

715

716

Figure 1.

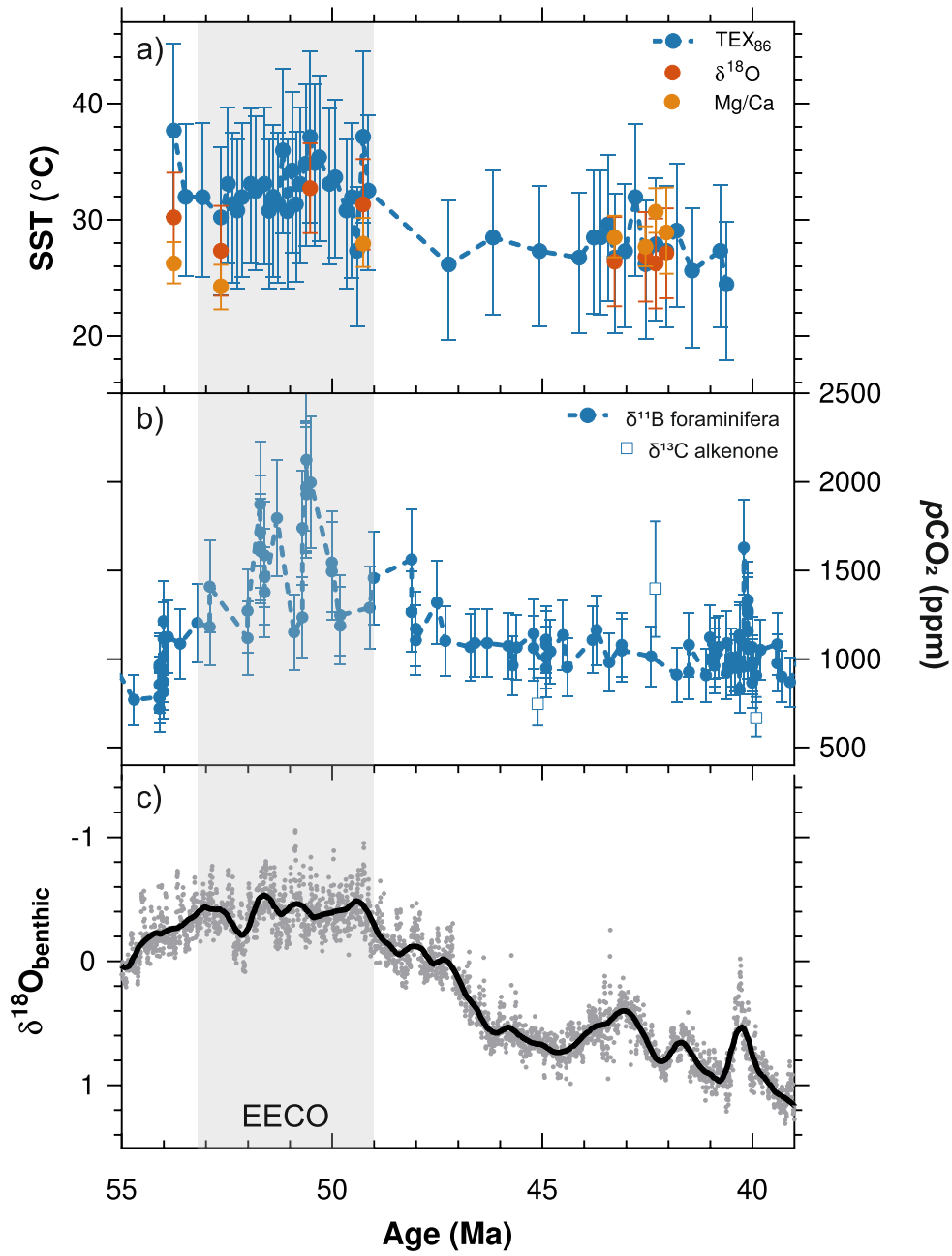


Figure 2.

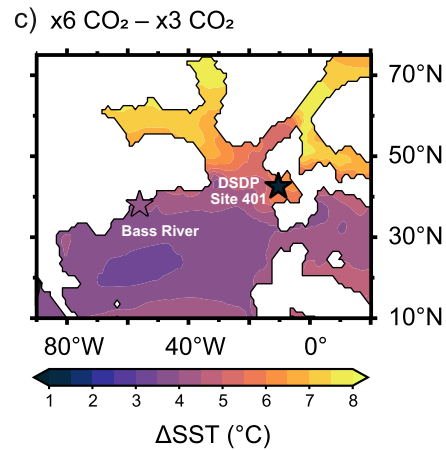
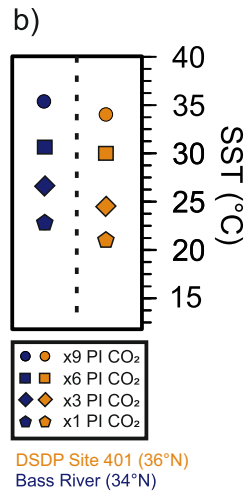
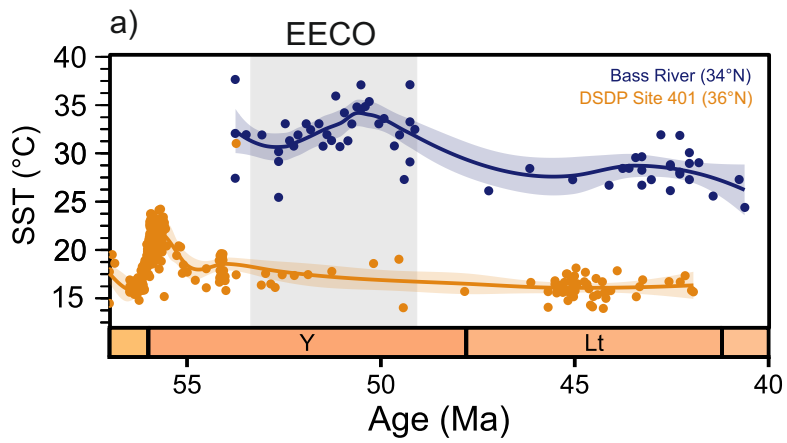


Figure 3.

EECO

